RSC Advances

PAPER

View Article Online
View Journal | View Issue

Cite this: *RSC Adv.*, 2024, **14**, 4034

Effect of hydrophobized PET TeMs membrane pore-size on saline water treatment by direct contact membrane distillation†

Arman B. Yeszhanov, *[ab] Ilya V. Korolkov,[ab] Olgun Güven,[c] Galina B. Melnikova,[d] Saule S. Dosmagambetova,[b] Alexander N. Borissenko,[e] A. K. Nurkassimov,[e] Murat T. Kassymzhanov[e] and Maxim V. Zdorovets[ab]

This paper describes the desalination process by membrane distillation (MD) using track-etched membranes (TeMs). Hydrophobic track-etched membranes based on poly(ethylene terephthalate) (PET TeMs) with pore diameters from 700 to 1300 nm were prepared by UV-initiated graft polymerization of lauryl methacrylate (LMA) inside the nanochannels. Modified PET TeMs were investigated by Fourier transform infrared (FTIR) spectroscopy, atomic force microscopy (AFM), scanning electron microscopy (SEM), thermogravimetric analysis (TGA) and contact wetting angle (CA) measurements. Hydrophobic PET TeMs were tested for treating saline solutions of different concentrations by the direct contact membrane distillation (DCMD) method. The influence of membrane pore diameter and salt solution concentration on the water flux and rejection degree were investigated. Membranes with CA 94 ± 4° were tested in the direct contact membrane distillation (DCMD) of 7.5–30 g L^{-1} saline solution. Hydrophobic membranes with large pore sizes showed water fluxes in the range of 1.88 to 11.70 kg m^{-2} h^{-1} with salt rejection values of up to 91.4%.

Received 2nd November 2023
Accepted 16th January 2024

DOI: 10.1039/d3ra07475g

rsc.li/rsc-advances

1 Introduction

Although more than seventy percent of the earth's surface is covered by rivers, lakes, seas and oceans, only slightly more than two percent of the world's water resources are potable. Most of the world's potable water is found in glaciers and groundwater, and a very small proportion in rivers and lakes.[1,2] In addition, modern industry and agriculture continue to pollute the natural environment with heavy metals, toxic and poisonous chemical compounds, nitrates and pesticides. With the rapid growth of the world's population and the development of industry, the shortage of good quality drinking water is becoming more acute every year.[3–5] Even more acute is the need to obtain drinking water by desalination of seas and oceans in coastal areas, and in arid desert areas with a minimum amount of fresh water. This explains the demand for and improvement in methods of desalinating seawater by removing high concentrations of salts.[6–10]

Various physical, biological, and chemical methods can be employed for treating seawater. The selection of a specific method depends on several factors, including treatment cost, chemical properties, installation space, and the potential generation of secondary pollution.[11–15] In response to these considerations, membrane technology is increasingly being incorporated into certain stages of water treatment processes.[16–19] Among the most well-known traditional methods of water desalination, such as electrodialysis,[20,21] direct and reverse osmosis,[22–25] nano-,[26,27] micro-,[28,29] ultrafiltration,[30,31] membrane distillation (MD) has prospects for widespread practical application due to the low operating temperature and pressure, high rejection of non-volatile components, and ability to use low-grade heat source.[32–34] Indeed, membrane distillation can be implemented in various configurations with different setups and designs.[35–40] One of the commonly used and cost-effective configurations is direct contact membrane distillation (DCMD).[41–44]

For successful application of a membrane in MD, the following requirements are imposed on it: membrane should be highly porous, thin and hydrophobic, allowing water vapor to be transferred from the initial solution (concentrate) to a clean side (permeate) with low thermal conductivity, while avoiding leakage of the salt solution.

[a]*The Institute of Nuclear Physics of the Republic of Kazakhstan, 050032 Almaty, Kazakhstan. E-mail: a.yeszhanov@inp.kz*

[b]*Laboratory of Engineering Profile, L. N. Gumilyov Eurasian National University, 010008 Astana, Kazakhstan*

[c]*Department of Chemistry, Hacettepe University, 06800 Ankara, Turkey*

[d]*A. V. Luikov Heat and Mass Transfer Institute of the National Academy of Sciences of Belarus, 220072 Minsk, Belarus*

[e]*JSC "Park of Nuclear Technologies", Kurchatova Str. 18/1, Kurchatov, Kazakhstan*

† Electronic supplementary information (ESI) available. See DOI: https://doi.org/10.1039/d3ra07475g

The most common polymers used in the manufacture of membranes for MD applications are poly(vinylidene fluoride) (PVDF), polytetrafluoroethylene (PTFE), polypropylene (PP) and polyethylene (PE).[45–48] Nevertheless, these membranes also come with certain disadvantages, including low productivity, elevated expenses, and fouling of the hydrophobic surface, all of which contribute to a decline in water purification efficiency. As a result, the exploration for alternative membrane types in the field of MD holds significant importance.

Track-etched membranes (TeMs) have been introduced into the MD process successfully.[49–53] These membranes offer several advantages, such as uniform pore geometry with controllable density per unit area, a well-distributed range of pore sizes with low tortuosity, and thin thickness. These features make TeMs highly appealing for use in accurate separation techniques.[54,55] Poly(ethylene terephthalate) (PET), polycarbonate (PC) films are the most commonly employed material for the production of TeMs.[56,57] As previously mentioned, hydrophobic properties are crucial for a membrane to be suitable for MD. However, PET TeMs exhibit medium-level hydrophobicity, which may not be sufficient for successful application in the MD process. For optimal performance in MD, membranes need to possess strong water-repellent properties.

Surface modification using hydrophobic agents is one of the methods used to increase the hydrophobicity of the membrane by changing the chemistry and morphology of the membrane surface. Graft polymerization and surface coating methods are mainly used as the simplest methods to increase the hydrophobicity of the membrane by depositing functional groups on the membrane surface.

In previous works, hydrophobic PET TeMs with pore diameters up to 400 nm were obtained by different methods such as surface coating and graft polymerization.[49–53] The MD process demonstrated a high salt rejection, but water flux performance was low. In this work, with the aim to reach higher flux, the hydrophobization of PET TeMs with large pore sizes by UV-initiated graft polymerization of lauryl methacrylate was considered.

2 Materials and methods

2.1. Materials

Benzophenone (BP), ethanol, lauryl methacrylate (LMA) (96%), sodium hydroxide, sodium chloride, acetic acid, *N*′*N*-dimethylformamide (DMF), 2-propanol, ethanol, and hexane were purchased from Sigma-Aldrich. By passing through an aluminum oxide chromatography column, the monomer was purified from the inhibitors. Solutions were prepared using deionized water (18.2 MΩ) obtained from the Akvilon D-301 water purification system.

2.2. Manufacturing and modification of track-etched membranes (TeMs)

Hostaphan® brand PET films manufactured by Mitsubishi polyester film (Germany) with a nominal thickness of 12 μm were irradiated with Kr ions with an average energy of 1.75 MeV per nucleon at a DC-60 heavy ion accelerator with a fluence of 1×10^6 ions per cm^2. Before chemical etching, the samples were photosensitized on both sides for 30 min. Photosensitization was carried out using an Osram OFR HNS 30W UV-C source with a wavelength of 254 nm and an intensity of 0.133 milliwatt cm^{-2}. The distance from the source to the sample was 10 cm. Chemical etching was carried out in 2.2 M NaOH at 85 °C for 6–12 min. After etching, the PET TeMs samples were stored in air at room temperature.

These conditions for obtaining track-etched membranes make it possible to obtain so-called cylindrical pores. However, according to,[58] inner pore radius is more than surface pore radius of nanochannels by around 8.5 nm (14%), measured by SAXS and SEM for membranes etched for 270 s with pore density of 1×10^9 pore per cm^2. We conventionally call the resulting channels cylindrical, but we mean that the shape of the channels can be somewhat different from perfect cylindrical one.[59]

The modification of PET TeMs was carried out by UV-initiated graft polymerization with lauryl methacrylate. First, 10×15 cm^2 samples were washed in deionized water to remove any pollution from the membrane surface. Then, the samples were dried in air at room temperature. Next, the dried samples were immersed in a 5% benzophenone solution in DMF for 24 h. After that, the membranes were quickly washed in ethanol and dried. Then, the samples were placed in a solution of lauryl methacrylate in 2-propanol with a concentration of 10–30% with the addition of 0.008 M benzophenone in 2-propanol. The solvent (2-propanol) was chosen due to its good solubility in the monomer as well as its UV transparency. The reaction mixture was purged with argon to remove dissolved oxygen. Graft polymerization was carried out under an OSRAM Ultra Vitalux E27 UV lamp (UVA: 315–400 nm, 13.6 W; UVB: 280–315 nm, 3.0 W) for 15–60 min. Next, the samples were washed in hexane to remove homopolymer and unreacted monomer from the PET TeMs surface, dried and weighed to determine the grafting degree.

2.3. Membrane characterization

FTIR spectra were recorded using an InfraLUM® FT-08 FTIR spectrometer with an ATR attachment (GladiATR, Pike) to study the chemical groups before and after modification. The measurements were carried out in the range from 400 to 4000 cm^{-1}, the number of scans was 32 at a temperature of 21–25 °C. The SpectraLUM® software was used to record the FTIR spectra. The hydrophobic properties of the modified PET TeMs were studied by measuring the water contact angle (CA). CA was measured at five different sample positions using a digital microscope with 1000× magnification by the static drop method at room temperature. The drop volume was 15 μL. Scanning electron microscope Hitachi TM 3030, and Atomic Force Microscope (AFM) (with a tip radius of 10 nm or less) Smart SPM-1000 AIST NT were used to characterize the morphology before and after modification of PET TeMs.

The surface elasticity modulus (E) was determined by using AFM data. This was accomplished by analyzing the approach

curves of the probe tip towards the sample surface, utilizing the static force spectroscopy mode and applying the Johnson–Kendall–Roberts model. This model accounts for both adhesion forces and the elastic deformation of the interacting objects. Additionally, the adhesion force (F_a) values were computed based on the probe tip's detachment from the sample surface.

The determination of the liquid entry pressure (LEP) followed the guidelines outlined in.[60,61] A circular sample with a radius of 1.25 cm was securely placed inside a sealed chamber, and a test was conducted using air with pressure gradually increasing. LEP assessment was performed using a pipette equipped with a capillary having a diameter of 0.7 mm.

2.4. Direct contact membrane distillation

The separation performance of hydrophobized PET TeMs was evaluated using direct contact membrane distillation (DCMD), as illustrated in Fig. 1. The DCMD system was equipped with four type-T thermocouples labeled as T1, T2, T3, and T4. The membrane was positioned within a cell designed for the MD process. Flow rates on the permeate and feed sides were controlled and maintained at a constant level of 227 ± 3 ml min^{-1} and 453 ± 3 ml min^{-1}, respectively. This regulation was achieved using the Easy load Cole-Parmer Masterflex L/s 77200-62. The temperature difference was consistently maintained at 70 °C.

Permeate flux and salt rejection were measured using a DCMD unit, which is presented and described in our previous work.[49,53] At fixed time intervals (30 s), the permeate flux was measured by weighing the mass of liquid collected on the permeate side. Aqueous NaCl solutions were used as the concentrate in DCMD. The concentrations ranged from 7.5 to 30 g L^{-1} for membranes with different pore sizes. Salinity rejection was calculated from change in conductivity measured by Hanna Instruments HI2030-01 (Cluj, Romania).

The water flux was estimated using the equation described in:[49,53]

$$Q = \frac{\Delta m}{S\Delta t} \quad (1)$$

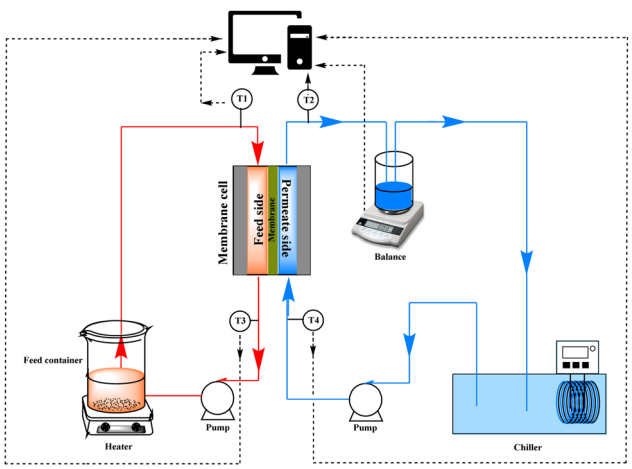

Fig. 1 Scheme of direct contact membrane distillation.

where Q – water flux (kg m^{-2} h^{-1}), Δm – mass of pure water on the permeate side (kg) per unit time Δt (h), S – the effective area of the membrane (m^2).

Salt rejection (R) was estimated using the following equation:

$$R = 100 - \left(\frac{C_{real}}{C_{fic}} \times 100\%\right) \quad (2)$$

$$C_{real} = \frac{\Delta\sigma \times 1000}{2.3} \quad (3)$$

$$C_{fic} = \frac{\Delta m \times C_{feed}}{m_p} \quad (4)$$

where R – degree of salt rejection, %; C_{real} – concentration of NaCl in the permeate side after MD, calculated according to conductivity (conductivity of 1 mg L^{-1} NaCl solution is 2.3 μS cm^{-1}), g L^{-1}; C_{fic} – theoretical concentration of NaCl (providing that the feed solution passed without purification), g L^{-1}; $\Delta\sigma$ – difference in conductivity of permeate solution before and after MD, μS cm^{-1}; 2300 μS cm^{-1} – change in the conductivity of the solution with addition of 1 g L^{-1} of NaCl; Δm – permeate gain after MD, g; C_{feed} – initial concentration of salt in feed solution, g L; m_p – mass of water from permeate side before MD, g.

3 Results and discussions

3.1. Preparation of hydrophobic membranes

UV-initiated graft polymerization, unlike other methods, has mild reaction conditions, low operating costs, and does not destroy the basic properties of substrates.

This method is based on the formation of radicals at the surface of the polymer with the help of photoinitiators that generate radicals under UV irradiation or sensitizers capable of tearing off a hydrogen atom from the polymer chain after transitioning to their excited state. The resulting radicals at the surface form nucleation centers of the polymer chain according to the free radical polymerization mechanism. The modification of PET TeMs was carried out following the procedure shown in Fig. 2.

Fig. 3 shows the effect of monomer concentration (A) and irradiation time (B) on grafting degree. It can be seen that the optimum condition for the reaction is for LMA concentration of 30%, with further increases in concentration leading to the increased formation of homopolymer. Increasing the irradiation time also affects the degree of grafting even leading to degradation of the PET TeMs surface. Thus, in Fig. 2b it can be seen that the grafting degree increases from 0.62% at 15 min to 6.84% at 60 min of irradiation. A further increase in irradiation time leads to the formation of homopolymer, overgrowth of the pore structure and degradation of the PET TeMs surface (the membrane become yellowish and fragile).

SEM was used to investigate the surface morphology of the pristine and modified PET TeMs. The results are shown in Table 1. SEM pictures of membrane surface are shown in Fig. 4, also SEM pictures from both sides of membranes are presented in Fig. S1.† From the SEM images, it can be seen that an increase

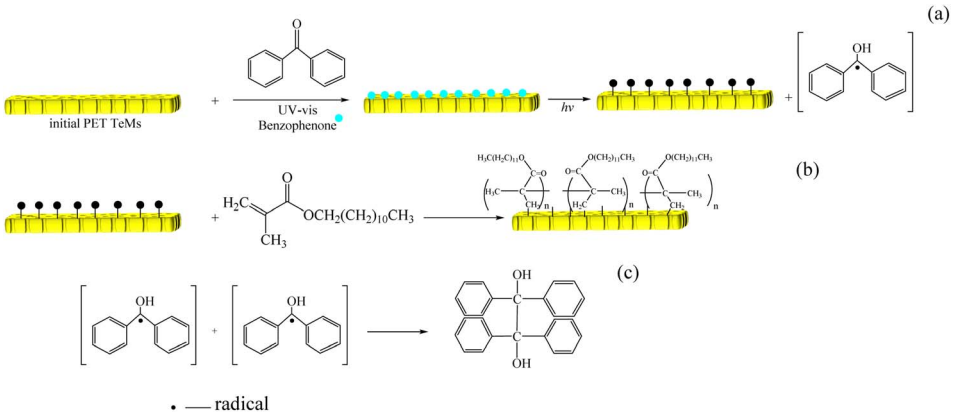

Fig. 2 Hydrophobization of PET TeMs by graft polymerization: (a) absorption of benzophenone on the surface of PET TeMs, (b) graft polymerization of lauryl methacrylate, (c) recombination of benzophenone.

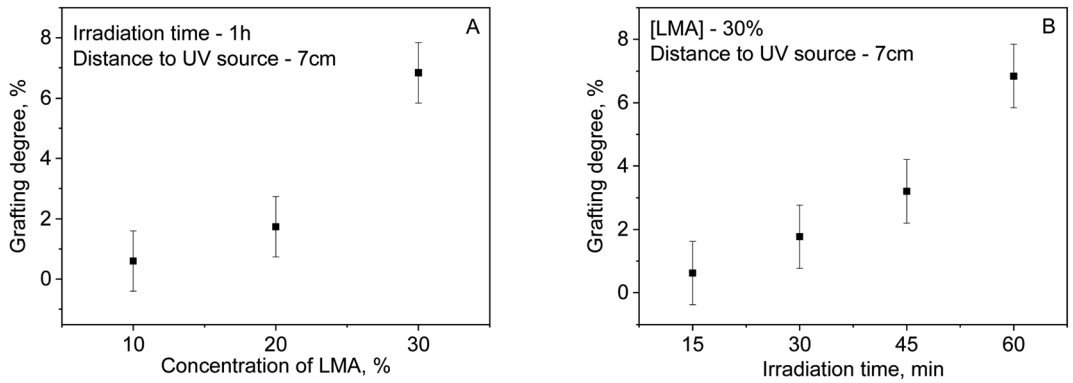

Fig. 3 Effect of monomer concentration and irradiation time on grafting degree of LMA on PET TeMs.

in the concentration of lauryl methacrylate leads to a gradual decrease in the pore size of the membranes. The pore size differs from different sides, but not more than 7%. According to SEM, pore size for Pristine PET TeMs is 1461 ± 39 nm, after modification with LMA with grafting degree of 6.84%, pore diameter decreased to 1305 ± 11 nm.

AFM was used to visualize the PET TeMs surface before and after modification, and to calculate the R_a, R_q and adhesion strength indices. Calculation of roughness (R_a, R_q), adhesion force and elasticity modulus was carried out using the equations used in.[62] The results are presented in Fig. 5 and Table 2. The roughness increased from 6.5 ± 1.3 nm to 16.7 ± 4.5 nm with the grafting process. The increase in roughness is associated with an increase in the amount of lauryl methacrylate grafted onto the surface of PET TeMs.

Fig. 6 shows the TGA curves of pristine PET TeMs and modified PET TeMs-*g*-PLMA with various degree of grafting. As shown in Fig. 6, there is an insignificant change in the behavior of the TGA weight loss curves as a result of the formation of very small amount of grafted layer of LMA, with the changes becoming little more pronounced with an increase in the grafting degree. In fact, this result shows that low level grafting

Table 1 Characteristics of PET TeMs before and after LMA modification (etching time – 12 min)

Sample type	Grafting time, min	Monomer concentration, %	Grafting degree, %	Pore size (SEM analysis), nm
Pristine PET TeMs	0	—	—	1461 ± 39
PET TeMs-*g*-PLMA	15	30	0.62	1436 ± 9
	30	30	1.77	1385 ± 6
	45	30	3.2	1349 ± 16
	60	10	0.6	1421 ± 13
	60	20	1.74	1373 ± 9
	60	30	6.84	1305 ± 11

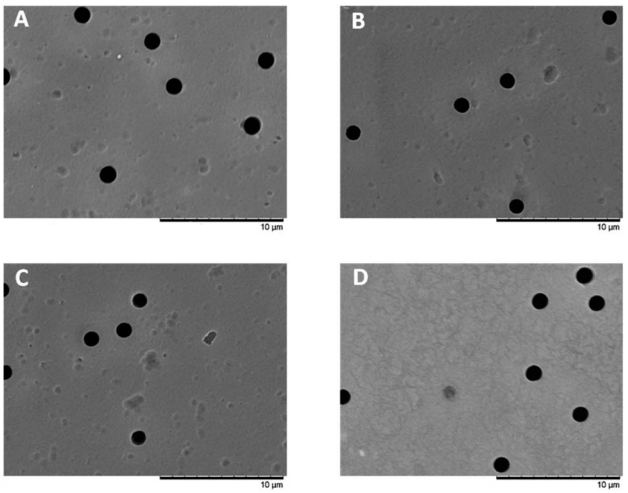

Fig. 4 SEM images of original PET TeMs (A), PET TeMs-*g*-PLMA (10%) (B), (20%) (C), (30%) (D).

of LMA on PET does not cause any adverse changes in the thermal stability of the original PET TeMs.

The evaluation of the hydrophobic properties was carried out by the method of water contact angle (CA) measurements. Fig. 7 and S2† show the results of CA measurements from 5 different positions of PET TeMs before and after graft polymerization. Increasing the grafting degree resulted in an increase in CA from 50–55° for pristine PET TeMs to 94° ± 4 for PET TeMs-*g*-PLMA with a degree of grafting of 6.84%.

Table 2 Results of atomic force microscopy of PET TeMs before and after LMA modification

Sample	R_a, nm	R_q, nm	E, MPa	F_a, nN
Pristine PET TeMs	6.5 ± 1.3	9.86 ± 3.0	129.0	64.9
PET TeMs-*g*-PLMA (10%)	6.7 ± 1.1	10 ± 1.3	100.7	67.1
PET TeMs-*g*-PLMA (20%)	7.0 ± 1.3	11.12 ± 2.6	125.4	58.5
PET TeMs-*g*-PLMA (30%)	16.7 ± 4.5	22.0 ± 5.9	47.71	103.2

An FTIR analysis was performed to confirm UV-graft polymerization and detect the presence of characteristic bands of poly(lauryl methacrylate) (PLMA) on the modified PET TeMs. FTIR spectra of both pristine and modified PET TeMs are presented in Fig. 8. The major absorption peaks of pristine PET TeMs are at 2972 cm^{-1} (aromatic CH), 2910 cm^{-1} (aliphatic CH), 1715 cm^{-1} (C=O), 1471 cm^{-1} (CH_2 bending), 1410 cm^{-1} (ring CH), 1341 cm^{-1} (CH_2 stretching), 1238 cm^{-1} (C=O–O stretching), 1018 cm^{-1} (ring CCC), 970 cm^{-1} (O–CH_2 stretching), 847 cm^{-1} (ring CC).[63] The presence of PLMA can be attributed to the appearance of CH groups detected at approximately 2860 cm^{-1} and 2925 cm^{-1}.

The liquid entry pressure (LEP) is the key factor in assessing water resistance in membrane processes. It denotes the minimum pressure needed to compel liquid through the

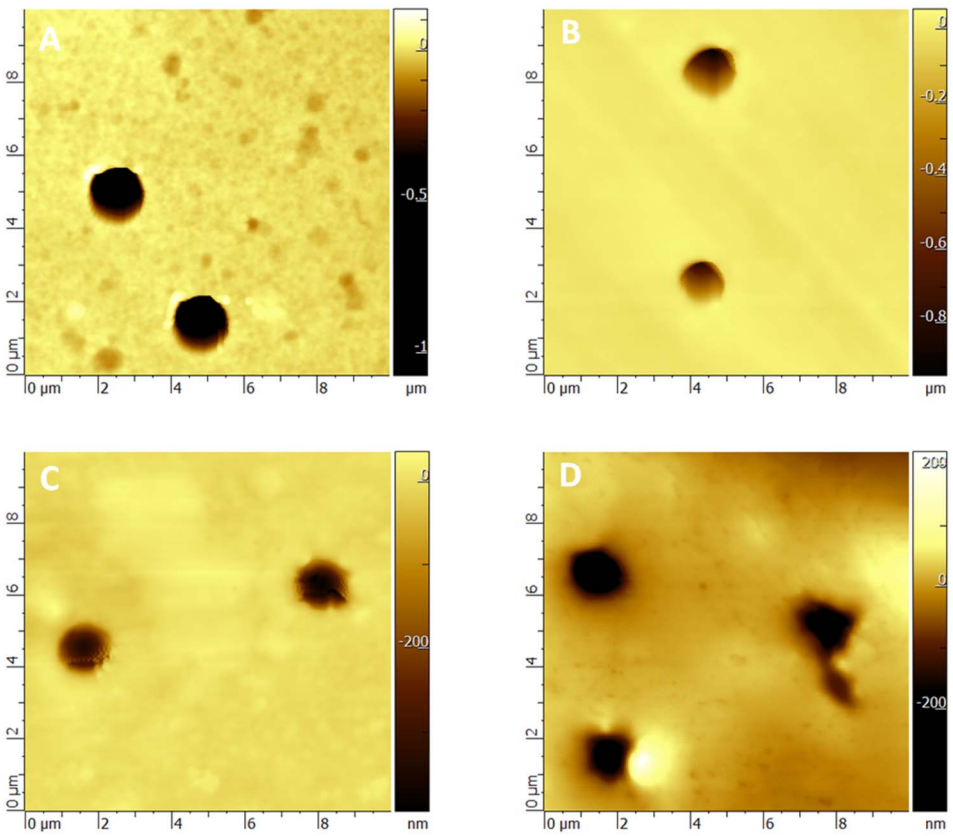

Fig. 5 AFM pictures of original PET TeM (A), PET TeMs-*g*-PLMA (10%) (B), (20%) (C), (30%) (D) (size 10 × 10 μm^2).

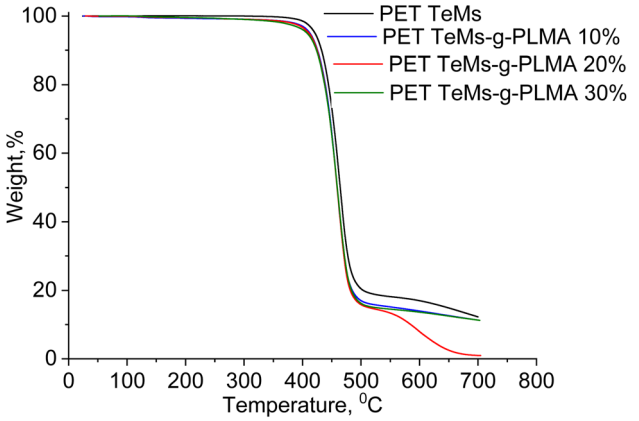

Fig. 6 TGA curves for a pristine PET TeMs and after grafting of LMA with various concentrations.

membrane's pores. The LEP is contingent upon the membrane's specific characteristics and can be calculated using the Laplace equation:[64]

$$\mathrm{LEP} = \frac{-2B\gamma_1 \cos(\theta)}{r_{\max}} \quad (5)$$

where B – the pore geometric coefficient (for cylindrical pores equal to one), γ_1 – the surface tension of the liquid, θ – the contact angle between the liquid and surface, $r_{\max}$ – the maximum pore size.

For aqueous solutions, membranes with a minimum LEP of 2.5 bar (or 0.25 MPa) are recommended for membrane distillation.[60] The membranes obtained under optimal conditions and different pore diameters showed the following LEP values: for 724 nm–>0.34 MPa, 1150 nm–0.145 MPa, 1305 nm–0.011 MPa. This means that membranes with a pore diameter of 724 nm can be used in MD.

3.2. Water treatment by direct contact membrane distillation

Membrane distillation of NaCl solutions (7.5–30 g L^{-1}) with hydrophobic PET TeMs prepared at optimal conditions (lauryl methacrylate – 30%, irradiation time – 60 min) with different pore diameters (742, 1150 and 1305 nm, obtained from pristine PET TeMs with pore sizes of 762, 1239 and 1461 nm) was performed in direct contact mode with temperature control.

The effect of membrane pore diameter and NaCl concentration on water flux and salt rejection was studied, the results are presented in Fig. 9. The results showed that there is a decrease in water flux with increasing salt concentration for all membranes of various pore diameters. For example, for membranes with a pore diameter of 724 nm, water flux decreased from 1.88 to 0.38 kg m^{-2} h^{-1} with an increase in salt concentration from 7.5 to 30 g L^{-1}. The increase in viscosity and partial pressure of the initial saline solution and the decrease in

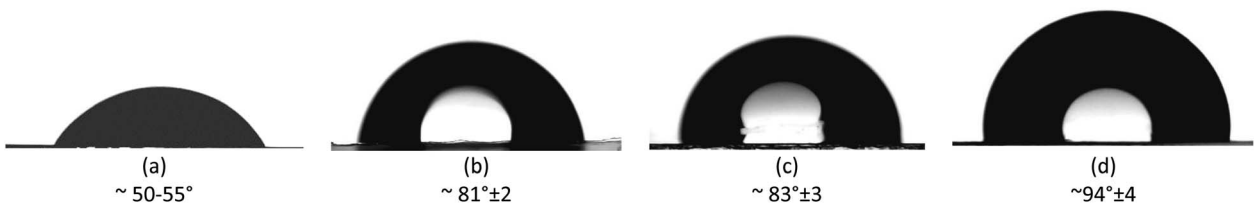

Fig. 7 CA of pristine PET TeM (a) and PET TeMs-*g*-PLMA with grafting degree of 0.6% (b), 1.74% (c) and 6.84% (d).

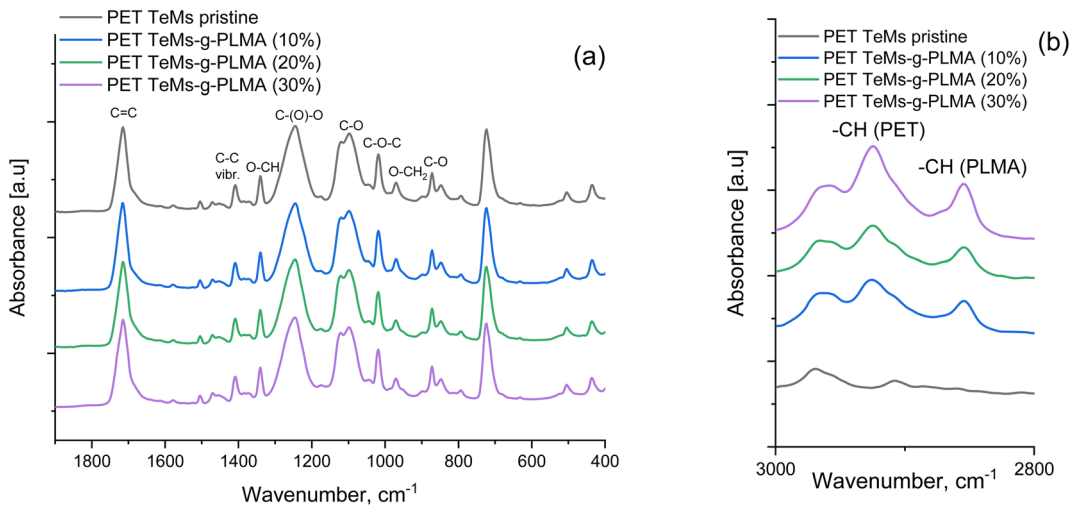

Fig. 8 FTIR spectra of pristine and modified PET TeMs-*g*-PLMA in the ranges of 1900–400 cm^{-1} (a), 3000–2800 cm^{-1} (b).

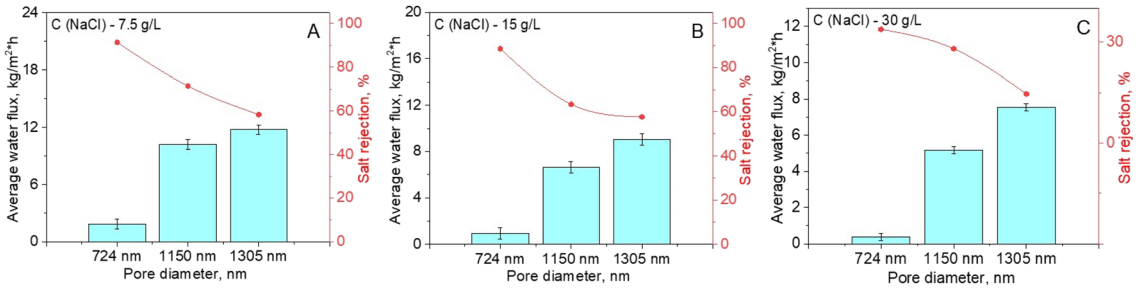

Fig. 9 Water flux and salt rejection during DCMD tests using hydrophobized PET TeMs-*g*-PLMA with different large pores for NaCl solutions with different concentrations.

water activity in the highly salty solution may explain the gradual dropping in water flux.

The salt rejection (R) was assessed by measuring the electrical conductivity of the purified solution using eqn (2)–(4). An appreciable rise in conductivity occurs as the NaCl concentration increases across all membranes with varying pore sizes. The effectiveness of salt rejection is significantly influenced by the size of the pores. An increase in pore diameter from 724 to 1305 nm led to a sharp decrease in the degree of purification from 91.39 to 58.35% at a salt concentration of 7.5 g L^{-1}. This is caused by a decrease in LEP values for pores with larger diameters, which can lead to salt leakage through the membrane.

4 Conclusion

In this study, we demonstrated a method for hydrophobizing the surface of PET TeMs with large pores by photoinitiated graft polymerization of lauryl methacrylate. The contact angle increased from ~50 to 94 ± 4° directly showing the hydrophobic modification of PET surface. SEM, TGA, AFM, and FTIR measurements confirmed the success of membrane modification. DCMD test showed average flux of 1.88 kg m^{-2} h^{-1} with degree of salt rejection of 91.39% at 7.5 g L^{-1} saline solution for membranes with pore diameters 720 nm. The obtained results demonstrate the significant potential of employing the resulting membranes with relatively large pore diameters in membrane distillation of saline solutions.

Abbreviations

TeMs	Track-etched membranes
PET	Poly(ethylene terephthalate)
PTFE	Polytetrafluoroethylene
PVDF	Poly(vinylidene fluoride)
PP	Polypropylene
LMA	Lauryl methacrylate
DCMD	Direct contact membrane distillation
SEM	Scanning electron microscope
FTIR	Fourier transform infrared spectroscopy
TGA	Thermogravimetric analysis
AFM	LEP atomic force microscopy liquid entry pressure

Author contributions

Conceptualization, A. B. Y., O. G. and M. V. Z.; methodology, I. V. K., G. B. M and S. S. D.; validation, A. N. B., N. A. A. and A. Ya.; formal analysis, I. V. K.; investigation, A. B. Y., A. K. N.; writing–original draft preparation, A. B. Y.; writing–review and editing, I. V. K., O. G., M. V. Z.; supervision, O. G. and S. S. D.; project administration, M. V. Z.; funding acquisition, M. V. Z., A. N. B., A. K. N., and M. T. K. All authors have read and agreed to the published version of the manuscript.

Conflicts of interest

The authors declare no conflict of interest.

Acknowledgements

The research titled "Development of methods for hydrophobization of PET track-etched membranes for water purification by membrane distillation" (grant no. AP14869096) was funded by the Ministry of Science and Higher Education of the Republic of Kazakhstan.

References

1 A. M. Bin *et al.*, *Desalination Technologies, Membrane Distillation, and Electrospinning, an Overview*, Elsevier, 2023. vol. 9, p. e12810.
2 M. K. Alsebaeai and A. L. Ahmad, Membrane distillation: Progress in the improvement of dedicated membranes for enhanced hydrophobicity and desalination performance, *J. Ind. Eng. Chem.*, 2020, **86**, 13–34.
3 Y. X. Lin, *et al.*, Preparation of PVDF/PMMA composite membrane with green solvent for seawater desalination by gap membrane distillation, *J. Membr. Sci.*, 2023, **679**, 121676.
4 C. Dong, Y. Huang and L. Zhang, Slug flow-enhanced vacuum membrane distillation for seawater desalination: Flux improvement and anti-fouling effect, *Sep. Purif. Technol.*, 2023, **320**, 124178.
5 H. Giraldo-Mejía, *et al.*, Plasma-grafting surface modifications to enhance membrane hydrophobicity for brine membrane distillation, *Desalination*, 2023, **567**, 116942.

6 M. M. Sayed, *et al.*, Environmentally friendly electrospun polycaprolactone bio-membrane fabrication for water distillation, *Mater. Today: Proc.*, 2023, DOI: 10.1016/j.matpr.2023.09.017.
7 J. Caspar, G. Xue and A. Oztekin, Performance characteristics on up-scaling vacuum membrane distillation modules, *Desalination*, 2023, 116994.
8 D. Liu, *et al.*, Liquid-lubricated nanofibrous membrane for scaling mitigation in solar-driven membrane distillation, *Sep. Purif. Technol.*, 2024, **329**, 125161.
9 H. R. Yang, *et al.*, Green fabrication of PVDF superhydrophobic membranes using a green solvent triethyl phosphate (TEP) for membrane distillation, *Desalination*, 2023, **566**, 116934.
10 M. Boukhriss, M. Timoumi and H. B. Bacha, Experimental of membrane distillation unit coupled with a DCMD using solar energy, *Sol. Compass.*, 2023, **7**, 100055.
11 V. T. Le, *et al.*, Sustainable cellulose-based hydrogels for water treatment and purification, *Ind. Crops Prod.*, 2023, **205**, 117525.
12 R. Peng, *et al.*, MOFs meet electrospinning: New opportunities for water treatment, *Chem. Eng. J.*, 2023, **453**, 139669.
13 A. H. Behroozi, M. Al-Shaeli and V. Vatanpour, Fabrication and modification of nanofiltration membranes by solution electrospinning technique: A review of influential factors and applications in water treatment, *Desalination*, 2023, **558**, 116638.
14 Y. Choi, *et al.*, Water management and produced water treatment in oil sand plant: A review, *Desalination*, 2023, **567**, 116991.
15 A. K. Inamdar, *et al.*, A review on environmental applications of metal oxide nanoparticles through waste water treatment, *Mater. Today: Proc.*, 2023, DOI: 10.1016/j.matpr.2023.05.527.
16 C. Tian, *et al.*, Recycling of end-of-life polymeric membranes for water treatment: Closing the loop, *J. Membr. Sci. Lett.*, 2023, **3**, 100063.
17 Z. Yang, C. Wu and C. Y. Tang, Making waves: Why do we need ultra-permeable nanofiltration membranes for water treatment?, *Water Res.: X*, 2023, **19**, 100172.
18 X. Liu, *et al.*, Recent progress of covalent organic frameworks membranes: Design, synthesis, and application in water treatment, *Eco Environ. Health*, 2023, **2**(3), 117–130.
19 U. Hani, Comprehensive review of polymeric nanocomposite membranes application for water treatment, *Alex. Eng. J.*, 2023, **72**, 307–321.
20 F. Alakhras, *et al.*, Diffusion analysis and modeling of kinetic behavior for treatment of brine water using electrodialysis process, *Water Sci. Eng.*, 2021, **14**(1), 36–45.
21 D. Ankoliya, *et al.*, Design and optimization of electrodialysis process parameters for brackish water treatment, *J. Clean. Prod.*, 2021, **319**, 128686.
22 X. Wu, *et al.*, Smart utilisation of reverse solute diffusion in forward osmosis for water treatment: A mini review, *Sci. Total Environ.*, 2023, **873**, 162430.
23 J. Wang and X. Liu, Forward osmosis technology for water treatment: Recent advances and future perspectives, *J. Clean. Prod.*, 2021, **280**, 124354.
24 V. R. Moreira, *et al.*, Low-cost recycled end-of-life reverse osmosis membranes for water treatment at the point-of-use, *J. Clean. Prod.*, 2022, **362**, 132495.
25 H. F. Giraldo Mejía, *et al.*, Direct recycling of discarded reverse osmosis membranes for domestic wastewater treatment with a focus on water reuse, *Chem. Eng. Res. Des.*, 2022, **184**, 473–487.
26 L. Yang, *et al.*, Bioinspired graphene oxide nanofiltration membranes with ultrafast water transport and selectivity for water treatment, *FlatChem.*, 2022, **36**, 100450.
27 A. Yuksekdag, *et al.*, Upgrading of conventional water treatment plant by nanofiltration for enhanced organic matter removal, *Sep. Purif. Technol.*, 2023, **325**, 124766.
28 A. Rajbongshi and S. B. Gogoi, Microfiltration, ultrafiltration and nanofiltration as a post-treatment of biological treatment process with references to oil field produced water of Moran oilfield of Assam, *Pet. Res.*, 2023, DOI: 10.1016/j.ptlrs.2023.09.001.
29 E. Virga, *et al.*, Theory of oil fouling for microfiltration and ultrafiltration membranes in produced water treatment, *J. Colloid Interface Sci.*, 2022, **621**, 431–439.
30 J. Lian, *et al.*, Mutual activation between ferrate and calcium sulfite for surface water pre-treatment and ultrafiltration membrane fouling control, *Sci. Total Environ.*, 2023, **858**, 159893.
31 M. Zambianchi, *et al.*, Graphene oxide-polysulfone hollow fibers membranes with synergic ultrafiltration and adsorption for enhanced drinking water treatment, *J. Membr. Sci.*, 2022, **658**, 120707.
32 M. Darman, N. Niknafs and A. Jalali, Effect of wavy corrugations on the performance enhancement of direct contact membrane distillation modules: A numerical study, *Chem. Eng. Process.: Process Intensif.*, 2023, **190**, 109421.
33 F. C. R. Costa, C. R. dos Santos and M. C. S. Amaral, Trace organic contaminants removal by membrane distillation: A review on mechanisms, performance, applications, and challenges, *Chem. Eng. J.*, 2023, **464**, 142461.
34 H. Julian, *et al.*, Membrane distillation for wastewater treatment: Current trends, challenges and prospects of dense membrane distillation, *J. Water Process. Eng.*, 2022, **46**, 102615.
35 T. Lee, *et al.*, Optimizing the performance of sweeping gas membrane distillation for treating naturally heated saline groundwater, *Desalination*, 2022, **532**, 115736.
36 S. Wang, *et al.*, Fouling mechanism and effective cleaning strategies for vacuum membrane distillation in brackish water treatment, *Desalination*, 2023, **565**, 116884.
37 Y. Tang, *et al.*, Superhydrophobic electrospun FPI/PTFE nanofiber membranes for robust vacuum membrane distillation, *Sep. Purif. Technol.*, 2023, **326**, 124856.
38 I. A. Said, *et al.*, Sweeping gas membrane distillation (SGMD) for wastewater treatment, concentration, and desalination: A

comprehensive review, *Chem. Eng. Process.: Process Intensif.*, 2020, **153**, 107960.

39 K. Ali, H. A. Arafat and M. I. Hassan Ali, Detailed numerical analysis of air gap membrane distillation performance using different membrane materials and porosity, *Desalination*, 2023, **551**, 116436.

40 C. Lai and H. Zhang, An efficient and economic evacuated U-tube solar collector powered air gap membrane distillation hybrid system for seawater desalination, *J. Clean. Prod.*, 2023, **394**, 136382.

41 J. Hu, *et al.*, Anisotropic gypsum scaling of corrugated polyvinylidene fluoride hydrophobic membrane in direct contact membrane distillation, *Water Res.*, 2023, **244**, 120513.

42 K. Ali, *et al.*, A numerical analysis of the electromagnetic field effect on direct contact membrane distillation performance, *Energy Convers. Manag.*, 2023, **292**, 117328.

43 J. Nambikkattu and N. J. Kaleekkal, Fluoroalkylsilane grafted FeOOH nanorods impregnated PVDF-co-HFP membranes with enhanced wetting and fouling resistance for direct contact membrane distillation, *J. Environ. Chem. Eng.*, 2023, **11**(3), 109624.

44 K. S. Chauhan and H. Tyagi, Thermal modeling of fluid flow and heat transfer in direct contact membrane distillation, *Energy Convers. Manag.*, 2023, **291**, 117249.

45 W. Tomczak, M. Gryta and K. Kowalczyk, The influence of storage time on the performance of polypropylene membranes applied for membrane distillation, *Sep. Purif. Technol.*, 2023, **308**, 122881.

46 J. Zhao, *et al.*, Preparation of PVDF/PTFE hollow fiber membranes for direct contact membrane distillation via thermally induced phase separation method, *Desalination*, 2018, **430**, 86–97.

47 H. Bazargan Harandi, *et al.*, Experimental and theoretical analysis of scaling mitigation for corrugated PVDF membranes in direct contact membrane distillation, *J. Membr. Sci.*, 2023, **686**, 122001.

48 J. Quan, *et al.*, Oriented shish-kebab like ultra-high molecular weight polyethylene membrane for direct contact membrane distillation, *Sep. Purif. Technol.*, 2022, **290**, 120847.

49 A. B. Yeszhanov, *et al.*, Recent Progress in the Membrane Distillation and Impact of Track-Etched Membranes, *Polymers*, 2021, **13**(15), 2520.

50 I. V. Korolkov, *et al.*, Modification of PET ion track membranes for membrane distillation of low-level liquid radioactive wastes and salt solutions, *Sep. Purif. Technol.*, 2019, **227**, 115694.

51 M. V. Zdorovets, *et al.*, Liquid low-level radioactive wastes treatment by using hydrophobized track-etched membranes, *Prog. Nucl. Energy*, 2020, **118**, 103128.

52 I. V. Korolkov, *et al.*, Preparation of PET track-etched membranes for membrane distillation by photo-induced graft polymerization//, *Mater. Chem. Phys.*, 2018, **205**, 55–63.

53 I. V. Korolkov, *et al.*, Modification of pet ion-track membranes by silica nanoparticles for direct contact membrane distillation of salt solutions, *Membranes*, 2020, **10**, 1–15.

54 A. A. Mashentseva, *et al.*, Application of silver-loaded composite track-etched membranes for photocatalytic decomposition of methylene blue under visible light, *Membranes*, 2021, **11**(1), 1–12.

55 N. Parmanbek, *et al.*, Environmentally friendly loading of palladium nanoparticles on nanoporous PET track-etched membranes grafted by poly(1-vinyl-2-pyrrolidone) via RAFT polymerization for the photocatalytic degradation of metronidazole, *RSC Adv.*, 2023, **13**(27), 18700–18714.

56 D. Temnov, *et al.*, Thermo-activation spectroscopy of track-etched membranes based on polyethylene terephthalate films irradiated by swift Xe ions, *Radiat. Phys. Chem.*, 2022, **191**, 109868.

57 A. Rossouw, *et al.*, Modification of polyethylene terephthalate track etched membranes by planar magnetron sputtered Ti/TiO2 thin films, *Thin Solid Films*, 2021, **725**, 138641.

58 S. Dutt, *et al.*, Shape of nanopores in track-etched polycarbonate membranes, *J. Membr. Sci.*, 2021, **638**, 119681.

59 P. Y. Apel, Fabrication of functional micro- and nanoporous materials from polymers modified by swift heavy ions// Radiat, *Phys. Chem.*, 2019, **159**, 25–34.

60 M. C. García-Payo, M. A. Izquierdo-Gil and C. Fernández-Pineda, Wetting study of hydrophobic membranes via liquid entry pressure measurements with aqueous alcohol solutions, *J. Colloid Interface Sci.*, 2000, **230**(2), 420–431.

61 A. Samadi, *et al.*, Engineering antiwetting hydrophobic surfaces for membrane distillation: A review, *Desalination*, 2023, **563**, 116722.

62 I. V. Korolkov, *et al.*, Preparation of Hydrophobic PET Track-Etched Membranes for Separation of Oil–Water Emulsion, *Membrane*, 2021, **11**(8), 637.

63 B. J. Holland and J. N. Hay, The thermal degradation of PET and analogous polyesters measured by thermal analysis-Fourier transform infrared spectroscopy, *Polymer*, 2002, **43**(6), 1835–1847.

64 S. Zare and A. Kargari, Membrane properties in membrane distillation, *Emerg. Technol. Sustain. Desalin. Handb*, Elsevier, 2018, pp. 107–156.